Materials Characterization 141 (2018) 318–327

Contents lists available at ScienceDirect

Materials Characterization

journal homepage: www.elsevier.com/locate/matchar

Effects of Mg-Al-O-Mn-S inclusion on the nucleation of acicular ferrite in magnesium-containing low-carbon steel

Chi-Kang Lin[a], Yan-Chi Pan[a], Yen-Hao Frank Su[b], Guan-Ru Lin[b], Weng-Sing Hwang[a], Jui-Chao Kuo[a,*]

[a] Department of Materials Science and Engineering, National Cheng Kung University, Taiwan
[b] Steelmaking Process Development Section, China Steel Corporation, Taiwan

ARTICLE INFO

Keywords:
Acicular ferrite
Nucleation mechanism
Inclusions
Low-carbon steel

ABSTRACT

The effects of inclusion size and chemical composition on acicular ferrite (AF) nucleation and possible nucleation mechanisms were discussed. With the use of low-carbon structure steel containing 13 ppm Mg, the chemical composition and size of inclusions were quantified by scanning electron microscopy combined with an energy dispersive spectroscopy system. Results showed that the complex inclusions MgO-MnS and MgO-Al_2O_3-MnS are the most effective inclusions for inducing AF nucleation in Mg-containing A36, and their probabilities of AF nucleation are 35.8% and 41.4%, respectively. Moreover, the inclusion size in the range of 1–2 μm exhibits the most remarkable ability to induce AF formation. AF nucleates at the interface of MgO and MgO-Al_2O_3 because of the low lattice misfit with AF. Complex inclusions, such as MgO-MnS and MgO-Al_2O_3-MnS, present a better ability of inducing AF formation than that of MnS due to the Mn-depleted zone.

1. Introduction

In general, the strength and the toughness of a heat-affected zone mainly depend on the grain size of the microstructure. The formation of acicular ferrite (AF) leads to a chaotic arrangement of ferrite plates in prior austenite and a fine grain structure [1]. In addition, the fine microstructure induced by the AF could inhibit the crack propagation and results in enhancing toughness [2,3]. AF formation depends on the following factors: chemical composition and alloy element of steels [4–6], grain size of prior austenite [7], cooling rate during austenite–ferrite transformation [8–13], and chemical composition and size distribution of nonmetallic inclusions [14–21].

Ti oxides [22], TiN, [23] and Al-Mn-O [24] are effective nucleation sites of AF, Moreover, the possible mechanisms of AF nucleation are given as follows. The complex inclusions together with precipitated MnS are the more active nucleation sites of AF than those of simple oxides with one phase [20,25]. The lattice misfit between the inclusion and α-ferrite should be low for the nucleation of AF [26] and the high thermal strain between the inclusion and steel will contribute to the nucleation of acicular ferrite [4].

Recently, the Mg-oxide metallurgy technology firstly proposed in 2004 reported that Mg oxides served to inhibit austenitic grain growth with the help of the pinning effect of oxides [27], because they are thermally stable to approximately 1673 K [28]. Mg-oxides, such as MgO, MgO-Al_2O_3, Ti_xO_y-MgO can also be nucleation sites for AF formation during austenite–ferrite transformation [29–31]. However, there exist different opinions on the ability of Mg containing inclusion to induce AF nucleation. It was reported that MgO or MgO-Al_2O_3 don't play a role at the formation of acicular ferrite [31,32]. The other researchers proposed that Mg containing inclusion can contribute to AF formation [33–35].

The previous studies have confirmed that Mg addition tended to promote the acicular ferrite nucleation in steel. But the possible mechanisms of IAF nucleation were not discussed in previous studies. Therefore, the mechanism of AF nucleation induced by Mg-containing inclusions was investigated in the present study.

2. Experimental

To understand the mechanism of AF nucleation induced by Mg-containing inclusions, A36 low-carbon steel with 13 ppm Mg was selected as experimental material. The chemical composition of the steel ingot is presented in Table 1. The molten steel was continuously cast into a slab with dimensions of 270 mm × 1800 mm × 8000 mm and subsequently machined into plates to remove the rust layers. Afterward, the plates were machined into cylindrical specimens (8 mm diameter

* Corresponding author.
E-mail addresses: cold19871025@gmail.com (C.-K. Lin), paino511@hotmail.com.tw (Y.-C. Pan), 150151@mail.csc.com.tw (Y.-H.F. Su), t120@mail.csc.com.tw (G.-R. Lin), wshwang@mail.ncku.edu.tw (W.-S. Hwang), jckuo@mail.ncku.edu.tw (J.-C. Kuo).

https://doi.org/10.1016/j.matchar.2018.05.005
Received 13 February 2018; Received in revised form 19 April 2018; Accepted 2 May 2018
Available online 03 May 2018
1044-5803/

Table 1
Chemical composition of A36 steel with 13 ppm Mg (wt%).

C	Si	Mn	P	S	N	O	Al	Mg
0.13	0.24	0.92	0.014	0.0035	0.0046	0.001	0.018	0.00132

and 3 mm height), polished, and ultrasonically cleaned by using a standard procedure for sample preparation. The prepared specimens were placed in a high-purity-aluminum crucible. The crucible was set on a high-temperature confocal laser scanning microscope (CLSM) equipped with an infrared image furnace. An in situ observation on the inclusion-induced AF formation was conducted using CLSM.

The specimen was heated to an austenitization temperature of 1573 K for 180 s to observe the austenite grain growth and continuously cooled down to 773 K at the cooling rate of 20 K/s to induce AF nucleation. After the heat treatment, the specimen was etched in 3% nital solution. Scanning electron microscopy (SEM) and energy dispersive spectroscopy (EDS) were used for microstructure observation and chemical composition profiling of the inclusions. The probability of AF nucleation P_{AF} is defined by the following:

$$P_{AF} = \frac{N_{AF}}{N_{total}} \times 100\%, \quad (1)$$

where 50 SEM micrographs of AF were randomly selected at 500× magnification, and N_{total} and N_{AF} are the total number of inclusions and number of inclusions with AF nucleation, respectively. Here, N_{total} and N_{AF} were measured in regard to nonmetallic inclusions with diameters higher than 1 μm due to the spatial limit of EDS.

Subsequently, the measured areas, including inclusions, and ferrite were selected and prepared for transmission electron microscopy (TEM) thin foil by using focused ion beam. The thin foil was observed using TEM at 200 kV. In addition, elemental analysis on the inclusions and the interface of the inclusions and matrix was performed using EDS.

Table 2
Number and number fraction of MnS, MgO-MnS, MgO, MgO-Al_2O_3-MnS, and MgO-Al_2O_3 in A36 steel containing 13 ppm Mg.

Inclusion type	MnS	MgO-MnS	MgO	Al_2O_3-MgO-MnS	Al_2O_3-MgO
Number	51	67	19	29	9
Distribution	29%	38%	11%	17%	5%

Table 3
Distribution of number and number fraction in terms of inclusion size for all measured inclusions in A36 steel containing 13 ppm Mg.

Inclusion size (μm)	1–2	2–3	3–4	4–5	5–10
Number	64	41	35	16	19
Distribution	38.8%	24.8%	21.2%	9.7%	11.5%

3. Results and Discussion

3.1. AF Formation

The in situ observation of ferrite transformation during cooling from 1573 K to 773 K at a cooling rate of 20 K/s is shown in Fig. 1. The inclusions appeared as small black dots in the CLSM micrographs, and the ferrite transformation occurred first at the austenite grain boundaries. Widmanstatten ferrite grew into austenite grains in the form of parallel-shaped plates. Ferrite nucleated on the inclusions-formed AF from 904 K to 810 K. AF only nucleated on specific inclusions, that is,

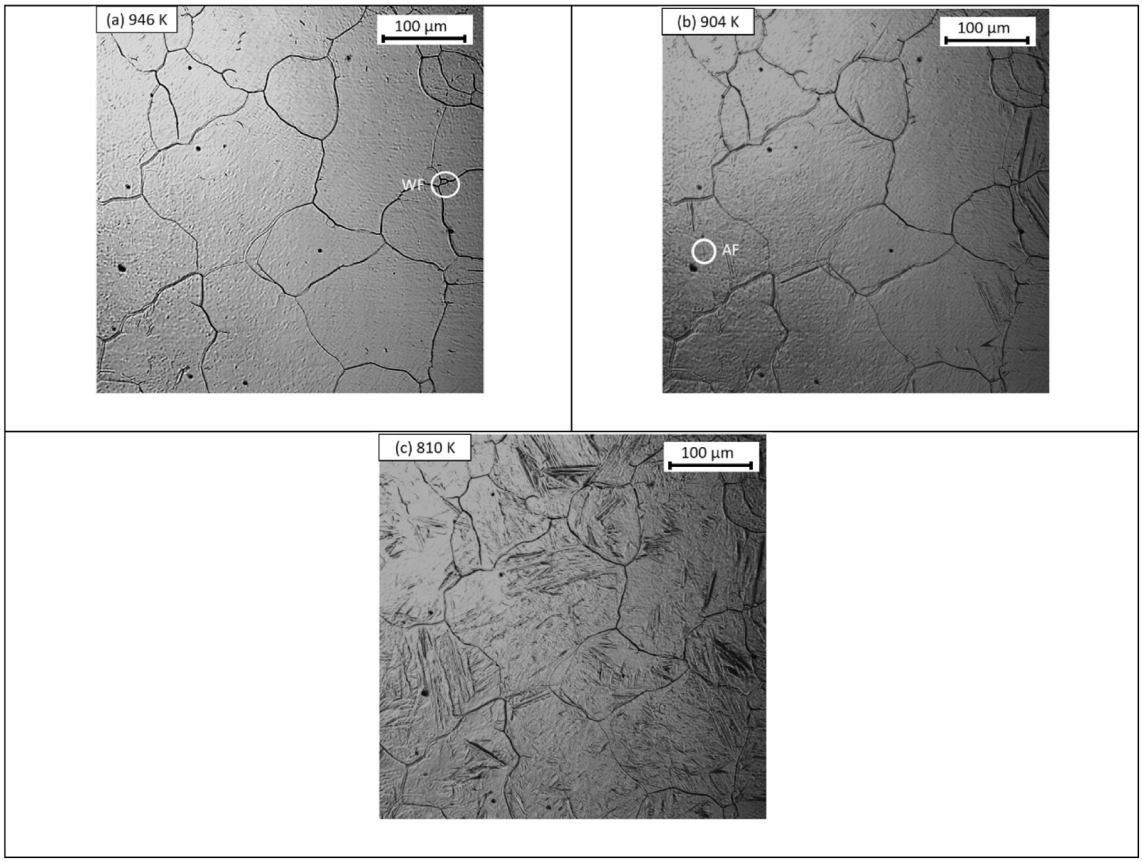

Fig. 1. In situ confocal laser scanning microscope micrographs (a) at the start of Widmanstatten ferrite (WF) nucleation, (b) at the start of acicular ferrite (AF) nucleation and (c) after the ferrite transformation at the cooling rate of 20 K/s in A36 steel with 13 ppm Mg.